KUNS1692

Symmetry-Unrestricted Skyrme-Hartree-Fock-Bogoliubov Calculations for Exotic Shapes in $N = Z$ Nuclei from ^{64}Ge to ^{84}Mo

M. Yamagami[1], K. Matsuyanagi[1] and M. Matsuo[2]

[1] *Department of Physics, Graduate School of Science, Kyoto University, Kyoto 606-8502, Japan*

[2] *Graduate School of Science and Technology, Niigata University, Niigata 950-2101, Japan*

Abstract

By performing fully 3D symmetry-unrestricted Skyrme-Hartree-Fock-Bogoliubov calculations, we discuss shape coexistence and possibility of exotic deformations simultaneously breaking the reflection and axial symmetries in proton-rich $N = Z$ nuclei: ^{64}Ge, ^{68}Se, ^{72}Kr, ^{76}Sr, ^{80}Zr and ^{84}Mo. Results of calculation indicate that the oblate ground state of ^{68}Se is extremely soft against the Y_{33} triangular deformation, and that the low-lying spherical minimum coexisting with the prolate ground state in ^{80}Zr may be unstable against the Y_{32} tetrahedral deformation.

PACS: 21.60-n; 21.60.Jz; 27.50.+e
Keywords: Hartree-Fock-Bogoliubov method; Skyrme interaction; Density-dependent pairing interaction; Shape coexistence; Non-axial octupole deformation; Proton-rich $N = Z$ nuclei

1 Introduction

The Hartree-Fock-Bogoliubov (HFB) method with the Skyrme interactions is one of the standard approaches in nuclear structure research [1,2]. In the last two decades it has become possible to solve the HFB equations directly in the coordinate mesh space [3,4]. In recent years, in order to investigate the structure of drip-line nuclei, the need for such coordinate-space HFB calculations has been greatly increased and intensive analyses have been made for neutron radii and skins in spherical neutron-rich nuclei [5–11]: Since the easier HF plus BCS method breaks down when treating the pairing correlation in weakly bound systems due to a leakage of nucleons into the continuum, we need to calculate the mean-field (particle-hole) correlations and the pairing (particle-particle) correlations selfconsistently in order to preserve confinement of the

nuclear density while allowing the pairing excitations to positive energy resonant states [3] (see, e.g. [12] and references therein for mean-field approaches other than the Skyrme-HFB method).

Recently, Terasaki, Heenen, Flocard and Bonche [13, 14] have removed the restriction of spherical symmetry in solving the coordinate-space Skyrme-HFB equations in order to investigate the possibility to get three-dimensional (3D) deformed solutions in neutron rich nuclei. In their works, a Skyrme interaction is used to describe the Hartree-Fock (HF) Hamiltonian while a density dependent zero-range interaction is used for the pairing channel. The mean-field HF equations are solved by the imaginary-time evolution method [15] in a 3D cubic mesh space while the HFB equations are solved in terms of the two-basis method developed earlier in [16, 17]. The discretization in 3D mesh space has the advantage over methods relying on an expansion in the harmonic-oscillator basis that nuclei with exotic deformations can be treated at the same level of accuracy [18–20]. In these works, however, reflection symmetries with respect to three planes are imposed for the nuclear density so that only one spatial octant is needed to solve the HFB equations.

The major purpose of this paper is to extend their method by removing the symmetry restrictions mentioned above and investigate the possibility of exotic shapes simultaneously breaking the axial and reflection symmetries in the mean field. For this purpose, we have constructed a new computer code that carries out Skyrme-HFB calculations in the 3D Cartesian-mesh space without imposing any restrictions on the spatial symmetry. Recently, on the basis of the Skyrme HF plus BCS calculations with no restriction on the nuclear shape, Takami, Yabana and Matsuo [21, 22] suggested that the oblate ground state of ^{68}Se is extremely soft against the Y_{33} triangular deformation, and that the low-lying "spherical" minimum coexisting with the prolate ground state in ^{80}Zr has the Y_{32} tetrahedral shape. As the first application of a fully 3D, symmetry-unrestricted Skyrme HFB method with the use of the density-dependent, zero-range pairing interaction [13, 14, 17, 23–30], we investigate in this paper shape coexistence and possibility of non-axial octupole deformations in proton rich $N = Z$ nuclei in the $A = 64 - 84$ region and examine the above predictions. These nuclei are especially interesting objects to study, since proton and neutron deformed shell effects act coherently and rich possibilities arise for coexistence and competition of different shapes (see [31] for earlier references). In recent years, active experimental studies of these nuclei are going on by means of combinations of radioactive nuclear beams and new gamma-ray and charged particle detector systems (see [32–35] for reviews). It should be noted here that, although extensive theoretical calculations and rich experimental evidences have been accumulated for axially symmetric octupole (Y_{30}) deformations, as reviewed in [36,37], only a few calculations using Woods-Saxon Strutinsky methods are available [38–41] except for light nuclei, and no firm experimental evidence exists up to now concerning the non-axial octupole (Y_{31}, Y_{32}, Y_{33}) deformations in the mean fields. For light nuclei, non-axial octupole deformations have been discussed [42–46] in connection with alpha-

cluster structures [47]; for instance, a triangular structure of ^{12}C [42,44] and a tetrahedral shape for ^{16}O [45,46].

Our motive for developing the coordinate-space Skyrme-HFB method is not only to investigate the possibilities of emergence of new types of symmetry breakdown in the ground states of proton-rich and neutron-rich nuclei, but also to investigate, in the future, low-lying modes of excitation of such unstable nuclei by means of the RPA and the Selfconsistent Collective Coordinate (SCC) method [48] on the basis of the HFB basis thus obtained. We intend to proceed in parallel with other calculations with the use of more phenomenological shell model potentials and separable interactions. The Skryme-HFB method is suited for this aim, as it provides a local mean-field potential so that such a comparative study is easy.

In Section 2, a brief account of the method of the coordinate-space Skyrme-HFB calculation is given. In Section 3, results of numerical calculation are presented and discussed. In Section 4, a conclusion is given.

2 Skyrme-HFB calculation

2.1 *Two basis method*

For convenience, we here recapitulate the two basis method [13, 14, 16, 17] adopted as the algorithm of our computer code. In this method, the imaginary-time evolution method is combined with a diagonalization of the HFB Hamiltonian matrix to construct the canonical basis.

We first determine the single-particle wave functions ϕ_i satisfying the HF equations

$$h\left[\rho\left(\boldsymbol{r}\right)\right]\phi_i\left(\boldsymbol{r}\right) = \varepsilon_i \phi_i\left(\boldsymbol{r}\right) \tag{1}$$

by means of the imaginary-time evolution method [15]. Here h, ε_i and $\rho(\boldsymbol{r})$ denote the mean-field Hamiltonian, the single-particle energies and the total nuclear density, respectively. (The isospin index τ is omitted for simplicity.) We next diagonalize the HFB Hamiltonian matrix [1]

$$\begin{pmatrix} h-\lambda & \Delta \\ -\Delta^* & -h^*+\lambda \end{pmatrix} \begin{pmatrix} U_k \\ V_k \end{pmatrix} = E_k \begin{pmatrix} U_k \\ V_k \end{pmatrix} \tag{2}$$

to get the one-body density matrix ρ and the pairing tensor κ:

$$\rho = V^* V^T, \quad \kappa = V^* U^T. \tag{3}$$

We then diagonalize the density matrix ρ and obtain the occupation coefficients n_α and the unitary transformation W which relates the HF wave functions ϕ_i to the canonical basis wave functions φ_α:

$$\rho_{kl} = \sum_{\alpha} n_{\alpha} W_{k\alpha} W^{\dagger}_{\alpha l} \tag{4}$$

$$\varphi_{\alpha}(\boldsymbol{r}) = \sum_{j} W_{j\alpha} \phi_{j}(\boldsymbol{r}). \tag{5}$$

In the canonical basis φ_{α}, the HFB density matrix in the coordinate space is diagonal:

$$\rho(\boldsymbol{r}, \boldsymbol{r}') = \sum_{\alpha} n_{\alpha} \varphi_{\alpha}(\boldsymbol{r}) \varphi_{\alpha}(\boldsymbol{r}')^{*}. \tag{6}$$

These steps are repeated until the convergence is achieved.

The single-particle wave functions and densities are represented on a full 3D Cartesian mesh space within a spherical container. In the present calculation, the radius of the spherical container and mesh spacing are set to $R_{mesh} = 10.0$ fm and $h = 1.0$ fm, respectively. Tajima et al. [49, 50] have carefully examined possible errors due to the use of the mesh size $h = 1.0$ fm and they found that, since discretization errors are essentially independent of the nuclear shape, deformation energies obtained with this mesh size are quite accurate (see also [51]). Actually, we have constructed the new Skyrme-HFB code by extending the cranked Skyrme-HF code [52] written previously and applied to the investigation of the yrast structure of ^{32}S, so that the cranking term can be included. In this paper, however, we examine only the cases of zero angular momentum.

2.2 *The Skyrme plus density-dependent pairing interactions*

We use the SIII parameter set [53] of the Skyrme interaction for the mean-field (particle-hole) channel, which has been successful in describing systematically the ground state quadrupole deformations in proton and neutron rich Kr, Sr, Zr and Mo isotopes [19] and in a wide area of nuclear chart [49]. For the pairing (particle-particle) channel, we use the density-dependent zero-range interaction [13, 14, 17, 23–30], which has been successful in describing, for instance, the odd-even staggering effects in charge radii,

$$V_{pair}(\boldsymbol{r}_1, \boldsymbol{r}_2) = \frac{V_0}{2} \left(1 - \hat{P}_{\sigma}\right) \left(1 - \frac{\rho(\boldsymbol{r}_1)}{\rho_c}\right) \delta(\boldsymbol{r}_1 - \boldsymbol{r}_2) \tag{7}$$

with the notation of [17], where the strength V_0 and the density ρ_c are parameters and $\hat{P}_{\sigma}$ denotes the spin exchange operator. For these parameters, we use the standard values [14, 17]: $V_0 = -1000.0$ MeV·fm^3, $\rho_c = 0.16$ fm^{-3}. The pairing interaction is smoothly cut off at 5 MeV above the Fermi energy in the

same way as in [19]. For a more general form of the density dependent pairing interaction, we refer [54, 55].

To check the dependence on the Skyrme-interaction parameter sets, we make calculations with the SkM* [56] and SLy4 [57] sets for an example of ^{68}Se. We refer to a recent work by Reinhard et al. [58] for a detailed and systematic study of shape coexistence phenomena in relation to the properties of various versions of the Skyrme interaction. We shall also check the dependence on the pairing strength V_0 adopted.

2.3 *Constrained HFB calculation*

In order to investigate the deformation properties away from the HFB equilibrium points, we perform constrained HFB calculations with the use of the quadratic constraints for the mass-quadrupole (octupole) moments [59] to obtain the energy surfaces as functions of the quadrupole (octupole) deformations. Because no spatial symmetry is imposed on the 3D mesh space, the center of mass and the directions of the principal axes of the nucleus can move freely without affecting the total energy. To evaluate the physical quantities like deformation parameters, it is crucially important to fulfill the constraints to keep the center of mass,

$$\left\langle \sum_{i=1}^{A} x_i \right\rangle = \left\langle \sum_{i=1}^{A} y_i \right\rangle = \left\langle \sum_{i=1}^{A} z_i \right\rangle = 0, \tag{8}$$

and the directions of the principal axes,

$$\left\langle \sum_{i=1}^{A} (xy)_i \right\rangle = \left\langle \sum_{i=1}^{A} (yz)_i \right\rangle = \left\langle \sum_{i=1}^{A} (zx)_i \right\rangle = 0. \tag{9}$$

These requirements are taken care of by means of the quadrupole constraints on these conditions as in our previous study [52].

2.4 *Deformation parameters*

As measures of the deformation, we calculate the mass-multipole moments,

$$\alpha_{lm} = \frac{4\pi}{3AR^l} \int r^l X_{lm}(\Omega)\, \rho(\boldsymbol{r})\, d\boldsymbol{r}, \quad (m = -l, \cdots, l) \tag{10}$$

where $\rho(\boldsymbol{r}) = \sum_{\alpha} v_\alpha^2 \left|\varphi_\alpha(\boldsymbol{r})\right|^2$, $R = 1.2A^{1/3}$ fm and X_{lm} are real bases of the spherical harmonics,

$$X_{l0} = Y_{l0}, \tag{11}$$

$$X_{l|m|} = \frac{1}{\sqrt{2}}(Y_{l-|m|} + Y^*_{l-|m|}), \tag{12}$$

$$X_{l-|m|} = \frac{-i}{\sqrt{2}}(Y_{l|m|} - Y^*_{l|m|}). \tag{13}$$

Here the quantization axis is chosen as the largest (smallest) principal axis for prolate (oblate) solutions. We then define the quadrupole deformation parameter β_2, the triaxial deformation parameter γ, and the octupole deformation parameters β_3 and β_{3m} by

$$\alpha_{20} = \beta_2 \cos\gamma, \quad \alpha_{22} = \beta_2 \sin\gamma, \tag{14}$$

$$\beta_3 = \left(\sum_{m=-3}^{3} \alpha_{3m}^2 \right)^{1/2}, \quad \beta_{3m} = \left(\alpha_{3m}^2 + \alpha_{3-m}^2 \right)^{1/2} \quad (m = 0, 1, 2, 3)\,. \tag{15}$$

For convenience, we also use the familiar notation $-\beta_2$ for oblate shapes with $(\beta_2, \gamma = 60^\circ)$.

3 Results and discussions

3.1 *Quadrupole deformations*

The solutions of the Skyrme-HFB equations obtained in the numerical calculations for ^{64}Ge, ^{68}Se, ^{72}Kr, ^{76}Sr, ^{80}Zr and ^{84}Mo are summarized in Table 1. The calculated ground-state shape changes from triaxial (^{64}Ge), oblate (^{68}Se, ^{72}Kr), large prolate (^{76}Sr, ^{80}Zr), to spherical shape (^{84}Mo) with increasing $N(= Z)$. For ^{68}Se, ^{72}Kr, ^{76}Sr, ^{80}Zr and ^{84}Mo, we obtain two or three local minima close in energy, indicating shape coexistence. These gross features are consistent with available experimental data [60–66] and previous theoretical calculations [19, 21, 22, 49, 67–77].

The potential energy curves obtained by the constrained HFB calculations are displayed in Fig. 1 as functions of the quadrupole deformation parameter β_2 and in Fig. 2 as functions of the triaxial deformation parameter γ. Below we remark on some specific points.

As seen in Fig. 2, the calculated potential energy curve for ^{64}Ge is rather shallow with respect to the γ degree of freedom so that this nucleus may be regarded as "γ-soft." This result is consistent with the experimental indication [60] and also with the shell model calculation by the Monte Carlo diagonalization method [75].

Quite recently, an excited prolate band coexisting with the ground-state oblate band has been found in ^{68}Se [63]. Their quadrupole deformations are

estimated as $\beta_2 \approx 0.27$ and $\beta_2 \approx -0.27$, respectively. Although the prolate excited band-head 0^+ state has not yet been observed, its excitation energy is estimated to be about 0.6 MeV. Our calculated energy difference between the prolate and the oblate HFB solutions, 0.52 MeV, is in good agreement with this experimental data. The barrier between the prolate and the oblate minima is about 3 MeV in the plot with respect to β_2 in Fig. 1, but it is only about 0.3 MeV in the plot with respect to the triaxial deformation parameter γ in Fig.2. It might be considered that, if the barrier is so low, the two bands built on the prolate and the oblate solutions interact strongly so that the shape coexistence picture is too much perturbed in contradiction with the experiment [63]. In our view, however, description of dynamics by going beyond the static mean-field approximation is necessary in order to discuss the interaction between the oblate and the prolate structures. In any case, understanding this shape coexistence dynamics is an interesting subject for future.

The second minimum with $\beta_2 \approx 0.66$ seen in the potential energy curve for ^{84}Mo in Fig. 1 may be regarded as a superdeformed solution, since it is related to the $Z = N = 42$ deformed shell gap [68] formed by occupying the down-sloping [431]1/2 levels from the upper major shell by two protons and two neutrons. This second minimum was also obtained in [21]. It offers an interesting possibility that a superdeformed rotational band might be observed at such a low excitation energy as about 1.5 MeV. From a viewpoint of deformed shell structure, the ground-state solutions for ^{76}Sr and ^{80}Zr have characteristics different from the second minimum in ^{84}Mo and may be distinguished from the superdeformation, although they have large prolate deformations of $\beta_2 \approx 0.5$.

3.2 *Non-axial octupole deformations*

As a result of the Skyrme-HFB calculations for proton-rich $N = Z$ nuclei from ^{64}Ge to ^{84}Mo (summarized in Table 1), we have found equilibrium shapes with finite non-axial octupole deformations for ^{68}Se and ^{80}Zr. The density distribution at the HFB local minimum for ^{68}Se with the triangular deformation superposed on the oblate shape and that for ^{80}Zr with the tetrahedral deformation are illustrated in Fig. 3.

In addition to the two cases mentioned above, Takami et al. [21] and Matsuo et al. [22] obtained, in their Skyrme-HF plus BCS calculations, finite equilibrium values of octupole deformations superposed on an oblate shape in ^{76}Sr and also on a near spherical shape in ^{84}Mo. According to their calculations, the potential-energy curves are very soft with respect to the octupole deformation degrees of freedom especially in the four cases mentioned above. In order to see the properties of the potential-energy curve in the neighborhood of the HFB equilibrium points and to make a better comparison with the results of Refs. [21, 22], we have carried out constrained HFB calculations with respect to the $\beta_{3m} (m = 0, 1, 2, 3)$ degrees of freedom for these four cases which are most interesting to us. Since the constrained HFB calculation is very time-

consuming, in this paper, we draw the potential-energy curve only for the four cases. We anticipate, however, that a more systematic calculation will soon become possible, considering a rapid progress of computer environments.

Figure 4 shows the potential-energy curves with respect to the octupole deformation parameters β_{3m} about the oblate shapes for ^{68}Se and ^{76}Sr, and about the spherical shapes for ^{80}Zr and ^{84}Mo. These curves are obtained by the constrained HFB calculations with the octupole operators $r^3 X_{3|m|}$ as constraints. We see that the oblate shape of ^{68}Se is unstable against the triangular (β_{33}) deformation and the spherical shape of ^{80}Zr is unstable against the tetrahedral (β_{32}) deformation, in good agreement with those of the Skyrme-HF plus BCS calculations of Refs. [21, 22], although local minima of potential energy curves are extremely shallow in our case. The oblate shape of ^{76}Sr is fairly soft with respect to the β_{32} and β_{33} deformations and the spherical ground state of ^{84}Mo is barely stable against all β_{3m} degrees of freedom, especially against β_{30}. In [22] an oblate solution with a finite equilibrium value of β_{32} is obtained for ^{76}Sr, while a similar solution for ^{76}Sr but with a finite equilibrium value of β_{33} and also a nearly spherical solution for ^{84}Mo with a finite equilibrium value of β_{30} is reported in [21]. Although such details differ depending on the treatment of the pairing correlations, the basic features, i.e., the softness to both β_{32} and β_{33} of the oblate shape of ^{76}Sr and the softess to β_{30} of the spherical shape of ^{84}Mo are in common between the present HFB calculations and those of [21, 22].

Below we focus our attention on the triangular deformation in ^{68}Se and the tetrahedral shape in ^{80}Zr and discuss about the microscopic origins of them.

Triangular deformation in ^{68}Se

Generally speaking, octupole correlations are associated with strong couplings between the shell-model orbits with $\Delta l = \Delta j = 3$ [36, 37]. In the $A = 64 - 84$ region under consideration, they are $1g_{9/2}$ and $2p_{3/2}$. In order to understand why the oblate shape in ^{68}Se is unstable (or extremely soft) against the triangular deformation, however, we need to examine the interplay of the quadrupole and octupole deformation effects. Namely, as explained below, the emergence of the triangular deformation is strongly correlated with the magnitude of the oblate deformation.

When ^{68}Se ($N = Z = 34$) is oblately deformed, the high Ω levels $[404]\frac{9}{2}$ and $[413]\frac{7}{2}$ stemming from the $1g_{9/2}$ orbit go down in energy and approach the Fermi surfaces for $N = Z = 34$ and strong Y_{33} couplings with $[301]\frac{3}{2}$ and $[310]\frac{1}{2}$ levels (associated with the $2p_{3/2}$ orbit) take place. These Y_{33} coupling effects are seen as repulsions between these levels in Fig. 5 which displays the neutron single-particle energies as functions of the triangular deformation parameter β_{33}. Here, the single-particle energies mean eigenvalues of the HF Hamiltonian with the density $\rho(\boldsymbol{r})$ determined by the HFB equations, and the asymptotic Nilsson quantum numbers are used only for convenience of labeling these levels: they are, of course, not good quantum numbers.

In this figure, results of calculation with use of the SkM* and SLy4 interactions are also shown for comparison. We note that the Y_{33} coupling effects are slightly weaker in the case of the SkM* and SLy4 interactions in comparison with the case of the SIII interaction. This is because the spacings between the levels coupled by the Y_{33} operator are the smallest for the SIII interaction: The spacings at the oblate equilibrium deformations between the [404]9/2 and [301]3/2 levels are about 2.8, 3.4 and 3.6 MeV, and those between the [413]7/2 and [310]1/2 levels are about 3.8, 4.1 and 4.2 MeV for the SIII, SkM* and SLy4 interactions, respectively. Thus, as shown in Fig. 6, the potential energy curve with respect to the triangular β_{33} deformation is softest for the case of the SIII interaction, although they are soft also for the cases of the SkM* and SLy4 interactions. Note that, in making this comparison, we have chosen the pairing-interaction strength V_0 such that the resulting pairing gaps Δ take about the same values for calculations with different Skyrme interactions (in order to make the effects of the pairing correlations approximately the same for all cases), as shown in the right-hand part of Fig. 6.

The importance of the triangular Y_{33} deformation superposed on the oblate shape was previously pointed out by Frisk, Hamamoto and May [78] in terms of a two-level model as well as the modified oscillator model which simulates the one-particle spectra in an infinite-well potential. Our result of the Skyrme-HFB calculation provides a realistic example which is consistent with their arguments.

Tetrahedral deformation in ^{80}Zr

As shown by Hamamoto, Mottelson, Xie and Zhang [79], the tetrahedral symmetry associated with the Y_{32} deformation brings about a bunching of the single-particle levels and create a remarkable shell structure: The $N = Z = 40$ is one of the magic numbers for such tetrahedral shapes. Such a shell effect is common to various finite Fermion systems, and in fact the tetrahedral deformation has been predicted, for instance, for sodium clusters consisting of 40 atoms by the density functional Kohn-Sham calculation [80,81], in which there is no spin-orbit coupling. The instability of the spherical shape of ^{80}Zr against the Y_{32} deformation, as exhibited in Fig. 4, is evidently connected to the magic number $N = Z = 40$ for the tetrahedral shape.

Figure 7 shows the single-particle energy diagrams as function of octupole deformation parameter $\beta_{3m} (m = 0, 1, 2, 3)$. As expected, we can see for the case of $m = 2$ a remarkable bunching of single-particle levels and an increase of the shell gap at $N = 40$ with increasing β_{32}, while the other octupole deformations $(m = 0, 1, 3)$ do not exhibit such a feature. Looking into details, one notices a fine splitting of the $1g_{9/2}$ level into three levels which correspond to irreducible representations of the double tetrahedral (spinor-T_d) group [41,45]; a twofold-degenerate level and two fourfold-degenerate levels.

Thus, the tetrahedral shell gap at $N = Z = 40$ emerges even under the presence of the strong spin-orbit coupling. It should also be noted that the

tetrahedral minimum is obtained in the calculation selfconsistently including the pairing correlations.

3.3 *Pairing gaps*

In this subsection, we first examine dependence of the pairing gaps on deformations, and then discuss about dependence of the non-axial octupole deformations on the pairing strength. The result of calculation for the pairing gaps at equilibrium deformations in each nucleus is listed in Table 1. As the pairing gaps in the HFB theory depend on single-particle levels, the numbers listed in this Table are averages of the diagonal elements in the HF basis, $\Delta_{i\bar{i}}$, over 5 MeV interval in the vicinity of the Fermi surfaces.

In the literatures, slightly different quantities like averages of the diagonal matrix elements in the canonical basis, $\Delta_{\alpha\bar{\alpha}}$, weighted by the coefficients of the Bogoliubov transformation, $u_\alpha v_\alpha$ [82–84] or v_α^2 [3], are used for similar purposes. Figure 8 compares these quantities for the case of triangular deformations superposed on the oblate shape in ^{68}Se. We see that the two average quantities, $\langle\Delta_{i\bar{i}}\rangle$ and $\langle\Delta_{\alpha\bar{\alpha}}u_\alpha v_\alpha\rangle$, are approximatelty equal. We also confirm that the averages do not significantly depend on the averaging interval.

Figures 9, 10 and 11 display the variation of the pairing gaps with the quadrupole deformation parameter β_2, the triaxial deformation parameter γ, and the octupole deformation parameters $\beta_{3m}(m = 0, 1, 2, 3)$, respectively. We observe that gross features of deformation dependence of the pairing gap correlate with the corresponding potential-energy curves displayed in Figs. 1, 2 and 4, respectively. Such correlations are rather easy to be understood from the behavior of the single-particle level density near the Fermi surface, i.e., from the well-known (spherical or deformed) shell effects that the level density near the Fermi surface becomes relatively low in the vicinities of the local minima of the potential energy curve [85]. Thus, the pairing correlation becomes weaker and the paring gap decreases near the local minima. On the other hand, the level density becomes relatively high and the pairing gap increases near the local maxima of the potential-energy curve.

Because of significant shape changes in the sequence of isotopes (isotones) in the $A = 64 - 84$ region, it is not always easy to extract the magnitudes of pairing correlations from experimental odd-even staggerings of binding energies and to assess the appropriateness of the pairing-interaction strength $V_0 = -1000$ MeV$\cdot$ fm^3 used in our HFB calculations. Quite recently, however, Satuła, Dobaczewski and Nazarewicz [86] have proposed a method for separating out the pairing correlation effects from the deformed mean-field (single-particle energy) effects on the odd-even staggerings, and evaluated average pairing gaps; these are in the range $1.0 - 1.6$ MeV for the mass region under consideration [87]. We note that these values agree rather well with the well-known global trend $\bar{\Delta} = 12/\sqrt{A}$ MeV [88], which are in the range $1.3-1.5$ MeV for $A = 64-84$. Our calculated values of the pairing gaps, listed in Table 1 and drawn in Figs. 9,10,11, mostly lie in this range of values, so that we

may say that the adopted strength for V_0 is reasonable.

Another possible source of ambiguity in evaluating the pairing gaps is the proton-neutron isoscalar pairings which are expected to play an important role in the $N = Z$ nuclei (see, for example, [89, 90] and references therein). We have assumed that such isoscalar pairings are absent in the states under consideration. Although this assumption should be examined, there are some experimental indications [90, 91] that this may be a fairly good approximation. It is clear that we need a more systematic and detailed investigations, both theoretical calculations and experimental explorations, for a better understanding of the pairing correlations in the proton-rich $N = Z$ nuclei in the $A = 64 - 84$ region.

In order to examine the sensitivity of the calculated results to the strength V_0 of the pairing interaction, we have made a calculation of the potential energy curve about the oblate shape in ^{68}Se as a function of the triangular octupole deformation parameter β_{33} for $V_0 = -900, -1000$ and -1100 MeV·fm^3. The result is shown in Fig. 12. As expected, the potential energy curve becomes shallower with increasing (absolute value of) V_0. Thus, the local minimum at $\beta_{33} \approx 0.10$ disappears with 10% increase of the (absolute) value of V_0. In any case, the potential is so shallow that we cannot associate a definite physical significance with the equilibrium values of β_{33}. We can still draw from these calculations an important conclusion that the oblate ground state of ^{68}Se is extremely soft with respect to the triangular octupole deformation.

3.4 *Discussions*

Actually, we need a more detailed investigation on the physical implication of the extremely soft potentials like those with respect to the triangular deformation in ^{68}Se and for the tetrahedral shape degree of freedom in ^{80}Zr. As is well known in the case of the axially symmetric Y_{30} octupole deformation [92–96], a definite minimum develops at finite value of β_{30} after the parity projection when the mean-field potential is very soft with respect to β_{30}. For the case of non-axial octupole deformations, a similar effect of the parity projection has been demonstrated by Takami, Yabana and Ikeda [42] for light nuclei. It remains to be examined whether or not the situation is similar for the non-axial octupole deformations in medium-mass nuclei under consideration.

More generally speaking, investigations of modes of excitation and of excitation spectra associated with the instabilities toward the non-axial octupole shape deformations is one of the major challenges for future. The present paper should be regarded as providing a HFB mean-field basis for a study of dynamics by means of methods like the quasiparticle RPA and the SCC method [48].

4 Conclusion

We have constructed a new computer code that carries out Skyrme-HFB calculations in the 3-dimensional Cartesian-mesh space without imposing any restriction on the spatial symmetry, and investigated shape coexistence and non-axial octupole deformations in proton-rich $N = Z$ nuclei, ^{64}Ge, ^{68}Se, ^{72}Kr, ^{76}Sr, ^{80}Zr and ^{84}Mo. The ground state shape changes from triaxial (^{64}Ge), oblate (^{68}Se, ^{72}Kr), large prolate (^{76}Sr, ^{80}Zr), to spherical (^{84}Mo) as $N(= Z)$ increases, in agreement with the available experimental data and the previous theoretical calculations. The instability toward the Y_{33} triangular deformation of the oblate ground state of ^{68}Se and that toward Y_{32} tetrahedral deformation of the excited spherical minimum of ^{80}Zr, pointed out by Takami et al. [21, 22] on the basis of the Skyrme-HF plus BCS calculations, have been confirmed by the fully selfconsistent Skyrme-HFB calculations with the use of the density-dependent zero-range pairing interaction.

The symmetry-unrestricted Skyrme-HFB computer code constructed in this work provides a selfconsistent mean-field basis for future investigation of collective modes of excitation in neutron-rich nuclei with neutron skins as well as in proton-rich nuclei.

Acknowledgements

During the course of this work, we have benefited from discussions with J. Dobaczewski, I. Hamamoto, P.-H. Heenen, S. Mizutori, W. Nazarewicz, H. Sagawa, N. Tajima, S. Takami, J. Terasaki, K. Yabana, and X.Z. Zhang. We would like to express our hearty thanks to them. The numerical calculations were performed on the NEC SX-4 supercomputers at Osaka University and at Yukawa Institute for Theoretical Physics, Kyoto University. This work was supported by the Grant-in-Aid for Scientific Research (No. 10640264) from the Japan Society for the Promotion of Science.

References

[1] P. Ring, P. Schuck, The Nuclear Many-Body Problem, Springer-Verlag, Berlin, 1980.

[2] S. Åberg, H. Flocard, W. Nazarewicz, Annu. Rev. Nucl. Part. Sci. 40 (1990) 439.

[3] J. Dobaczewski, H. Flocard, J. Treiner, Nucl. Phys. A 422 (1984)103.

[4] A. Bulgac, Preprint FT-194-1980, Bucharest, 1980: nucl-th/9907088.

[5] R. Smolańczuk, J. Dobaczewski, Phys. Rev. C 48 (1993) R2166.

[6] J. Dobaczewski, W. Nazarewicz, T.R. Werner, Z. Phys. A 354 (1996) 27.

[7] J. Dobaczewski, W. Nazarewicz, T.R. Werner, J.F. Berger, C.R. Chinn, J. Dechargé, Phys. Rev. C 53 (1996) 2809.

[8] S. Mizutori, J. Dobaczewski, G.A. Lalazissis, W. Nazarewicz, P.-G. Reinhard, Phys. Rev. C 61 (2000) 044326.

[9] P.-G. Reinhard, M. Bender, K. Rutz, J. A. Maruhn, Z. Phys. A 358 (1997) 277.

[10] N. Tajima, in: H. Horiuchi, M. Kamimura, H. Toki, F. Fujiwara, M. Matsuo, Y. Sakuragi (Eds.), Proc. Int. Symp. on Innovative Computational Methods in Nuclear Many-Body Problems, Osaka, Japan, November 10-15, 1997, World Scientific, Singapore, 1998, p. 343.

[11] N. Tajima, in: Proc. Int. Symp. on Models and Theories of the Nuclear Mass, Wako, Japan, July 19-23, 1999, RIKEN Review 26 (2000) 87.

[12] Jie Meng, Nucl. Phys. A 635 (1998) 3.

[13] J. Terasaki, P.-H. Heenen, H. Flocard, P. Bonche, Nucl. Phys. A 600 (1996) 371.

[14] J. Terasaki, H. Flocard, P.-H. Heenen, P. Bonche, Nucl. Phys. A 621 (1997) 706.

[15] K.T.R. Davies, H. Flocard, S.J. Krieger, M.S. Weiss, Nucl. Phys. A 342 (1980) 111.

[16] B. Gall, P. Bonche, J. Dobaczewski, H. Flocard, P.-H. Heenen, Z. Phys. A 348 (1994) 183.

[17] J. Terasaki, P.-H. Heenen, P. Bonche, J. Dobaczewski, H. Flocard, Nucl. Phys. A 593 (1995) 1.

[18] H. Flocard, P.H. Heenen, S.J. Krieger, M.S. Weiss, Nucl. Phys. A 391 (1982) 285.

[19] P. Bonche, H. Flocard, P. -H. Heenen, S. J. Krieger, M. S. Weiss, Nucl. Phys. A 443 (1985) 39.

[20] P. Bonche, H. Flocard, P.H. Heenen, Nucl. Phys. A 467 (1987) 115.

[21] S. Takami, K. Yabana, M. Matsuo, Phys. Lett. B 431 (1998) 242.

[22] M. Matsuo, S. Takami, Y. Yabana, in: C. Baktash (Ed.) Proc. Int. Conf. on Nuclear Structure '98, Gatlinburg, TN, August 10-15, 1998, AIP Conference Proceedings 481, American Institute of Physics, New York, 1999, p. 345

[23] R.R. Chasman, Phys. Rev. C 14(1976) 1935.

[24] G.F. Bertsch, H. Esbensen, Ann. Phys. 209(1991) 327.

[25] V.E. Starodubsky, M.V. Zverov, Phys. Lett. B 276 (1992) 269.

[26] N. Tajima, P. Bonche, H. Flocard and P.-H. Heenen, M.S. Weiss, Nucl. Phys. A 551 (1993) 434.

[27] D. Zawischa, U. Regge, R. Stapel, Phys. Lett. B 185 (1987) 299.

[28] U. Regge, D. Zawischa, Phys. Rev. Lett. 61 (1988) 149.

[29] S.A. Fayans, S.V. Tolokonnikov, E.L. Trykov, D. Zawischa, Phys. Lett. B338 (1994) 1.

[30] I.N. Borzov, S.A. Fayans, E. Krömer, D. Zawischa, Z. Phys. A 355 (1996) 117.

[31] J. Eberth, R.A. Meyer, K. Sisteich (Eds), Nuclear Structure of the Zr region, Springer, Berlin, 1988.

[32] J. Simpson, Nucl. Phys. A 654 (1999) 178c.

[33] W. Nazarewicz, Ncl. Phys. A 654 (1999) 195c.

[34] A. C. Mueller, Nucl. Phys. A 654 (1999) 215c.

[35] I. Tanihata, Nucl. Phys. A 654 (1999) 235c.

[36] I. AhmadCP.A. Butler, Annu. Rev. Nucl. Part. Sci. 43 (1993) 71.

[37] P.A. Butler, W. Nazarewicz, Rev. Mod. Phys. 68 (1996) 349.

[38] J. Skalski, Phys. Rev. C 43 (1991) 140.

[39] R.R. Chasman, Phys. Lett. B 266 (1991) 243.

[40] X. Li, J. Dudek, P. Romain, Phys. Lett. B 271 (1991) 281.

[41] X. Li, J. Dudek, Phys. Rev. C 49 (1994) R1250.

[42] S. Takami, K. Yabana, K. Ikeda, Prog. Theor. Phys. 96 (1996) 407.

[43] G. Leander, S.E, Larsson, Nucl. Phys. A 239 (1975) 93.

[44] J. Eichler, A. Faessler, Nucl. Phys. A 157 (1970) 166.

[45] N. Onishi and R.K. Sheline, Nucl. Phys. A 165 (1971) 180.

[46] J.P. Elliott, J.A. Evans, E.E. Maqueda, Nucl. Phys. A 437 (1985) 208.

[47] Y. Fujiwara, H. Horiuchi, K. Ikeda, M. Kamimura, K. Katō, Y. Suzuki, E. Uegaki, Suppl. Prog. Theor, Phys. 68 (1980) 29.

[48] T. Marumori, T. Maskawa, F. Sakata, A. Kuriyama, Prog. Theor. Phys. 64 (1980) 1294.

[49] N. Tajima, S. Takahara, N. Onishi, Nucl. Phys. A 603 (1996) 23.

[50] S. Takahara, N. Tajima, N. Onishi, Nucl. Phys. A 642 (1998) 461.

[51] P. Hoodbhoy, J.W. Negele, Nucl. Phys. A 288 (1977) 23.

[52] M. Yamagami, K. Matsuyanagi, Nucl. Phys. A 672 (2000) 123.

[53] M. Beiner, H. Flocard, Nguyen van Giai, P. Quentin, Nucl. Phys. A 238 (1975) 29.

[54] S.A. Fayans, D. Zawischa, Phys. Lett. B 383 (1996) 19.

[55] S.A. Fayans, S.V. Tolokonnikov, E.L. Trykov, D. Zawischa, Nucl. Phys. A 676 (2000) 49.

[56] J. Bartel, P. Quentin, M. Brack, C. Guet, H.-B. Håkansson, Nucl. Phys. A 386 (1982) 79.

[57] E. Chabanat, P. Bonche, P. Haensel, J. Meyer, R. Schaeffer, Nucl. Phys. A 627 (1997) 710; Nucl. Phys. A 635 (1998) 231.

[58] P.-G. Reinhard, D.J.Dean, W. Nazarewicz, J. Dobaczewski, J.A. Maruhn, M.R. Strayer, Phys. Rev. C 60 (1999) 014316.

[59] H. Flocard, P. Quentin, A.K. Kerman, D. Vautherin, Nucl. Phys. A 203 (1973) 433.

[60] P.J. Ennis, C.J. Lister, W. Gelletly, H.G. Price, B.J. Varley, P.A. Butler, T. Hoare, S. Ćwiok, W. Nazarewicz, Nucl. Phys. A 535 (1991) 392.

[61] C.J. Lister, P.J. Ennis, A.A. Chishti, B.J. Barley, W. Gellely, H.G. Price, A.N. James, Phys. Rev. C 42 (1990) R1191.

[62] S. Skoda, B. Fiedler, F.Becker, J. Eberth, S.Freund, T. Steinhardt, O. Stuch, O. Thelen, H.G. Thomas, L. Käubler, J. Reif, H. Schnare, R. Schwengner, T. Servene, G. Winter, V. Fischer, A. Jungclaus, D. Kast, K.P. Lieb, C. Teich, C. Ender, T.Härtlein, F. Köck, D. Schwalm, P.Baumann, Phys. Rev. C 58 (1998) R5.

[63] S.M. Fischer, D.P. Balamuth, P.A. Hausladen, C.J. Lister, M.P. Carpenter, D. Seweryniak, J. Schwartz, Phys. Rev. Lett. 84 (2000) 4064.

[64] G. de Angelis, C. Fahlander, A. Gadea, E. Farnea, W. Gelletly, A. Aprahamian, D. Bazzacco, F. Becker, P.G. Bizzeti, A. Bizzeti-Sona, F. Brandolini, D. de Acuna, M. De Poli, J. Eberth, D. Foltescu, S.M. Lenzi, S. Lunardi, T. Martinez, D.R. Napoli, P. Pavan, C.M. Petrache, C. Rossi Alvarez, D. Rudolph, B. Rubio, W. Satula, S. Skoda, P. Spolaore, H.G. Thomas, C.A. Ur, R. Wyss, Phys. Lett. B 415 (1997) 217.

[65] C.J. Lister, M. Campbell, A.A. Chishti, W. Gelletly, L. Goettig, R. Moscrop, B.J. Varley, A.N. James, T. Morrison, H.G. Price, J. Simpson, K. Connell, O. Skeppstedt, Phys. Rev. Lett. 59 (1987) 1270.

[66] D. Bucurescu, C. Rossi Alvarez, C.A. Ur, N. Marginean, P. Spolaore, D. Bazzacco, S. Lunardi, D.R. Napoli, M. Ionescu-Bujor, A. Iordachescu, C.M. Petrache, G. de Angelis, A. Gadea, D. Foltescu, F. Brandolini, G. Falconi, E. Farnea, S.M. Lenzi, N.H. Medina, Zs. Podalyak, M. De Poli, M.N. Rao, R. Venturelli, Phys. Rev. C 56 (1997) 2497.

[67] K. Hyde, J. Moreau, M. Waroquier, Phys. Rev. C 29 (1984) 1859.

[68] W. Nazarewicz, J. Dudek, R. Bengtsson, T. Bengtsson, I. Ragnarsson, Nucl. Phys. A 435 (1985) 397.

[69] J. Dudek, W. Nazarewicz, N. Rowley, Phys. Rev. C 35 (1987) 1489.

[70] J.P. Maharana, Y.K. Gambhir, J.A. Sheikh, P. Ring, Phys. Rev. C 46 (1992) R1163.

[71] E Kirchuk, P. Federman, S. Pittel, Phys. Rev. C 47 (1993) 567.

[72] G.A. Lalazissis, M.M. Sharma, Nucl. Phys. A 586 (1995) 201.

[73] A. Petrovici, K.W. Schmid, A. Faessler, Nucl. Phys. A 605 (1996) 290.

[74] A. Petrovici, K.W. Schmid, A. Faessler, Nucl. Phys. A 665 (2000) 333.

[75] M. Honma, T. Mizusaki, T. Otsuka, Phys. Rev. Lett. 77 (1996) 3315.

[76] I. Hamamoto, X.Z. Zhang, Z. Phys. A 353 (1995) 145.

[77] P. Sarriguren, E. Moya de Guerra, A. Escuderos, Nucl. Phys. A 658 (1999) 13.

[78] F. Frisk, I. Hamamoto, F.R. May, Phys. Scr. 50 (1994) 628.

[79] I. Hamamoto, B. Mottelson, H. Xie, X.Z. Zhang, Z. Phys. D 21 (1991) 163.

[80] S.M. Reimann, M. Koskinen, H. Häkkinen, P.E. Lindelof, M. Manninen, Phys. Rev. B 56 (1997) 12147.

[81] J. Kolehmainen, M. Koskinen, H. Häkkinen, M. Manninen Czechoslovak J. of Phys. 48 (1998) 679.

[82] S. Takahara, N. Onishi, N. Tajima, Phys. Lett. B 331 (1994) 261.

[83] M. Bender, K. Rutz, P.-G. Reinhard, J. A. Maruhn, arXiv:nucl-th/0005028.

[84] T. Duguet, P. Bonche, P.-H. Heenen, arXiv:nucl-th/0005040.

[85] M. Brack, Jens Damgaad, A.S. Jensen, H.C. Pauli, V.M. Strutinsky, C.Y. Wong, Rev. Mod. Phys. 44 (1972) 320.

[86] W. Satuła, J. Dobaczewski, W. Nazarewicz, Phys. Rev. Lett. 81 (1998) 3599.

[87] J. Dobaczewski, P. Magierski, W. Nazarewicz, W. Satula, Z. Szymański, arXiv:nucl-th/0003019.

[88] A. Bohr, B.R. Mottelson, Nuclear Structure, Vol. I, Single-Particle Motion, Benjamin, 1969.

[89] W. Satuła, D.J. Dean, J. Gary, S. Mizutori, W. Nazarewicz, Phys. Lett. B 407 (1997) 103.

[90] A.O. Macchiavelli, P. Fallon, R.M. Clark, M. Cromaz, M.A. Deleplanque, R.M. Diamond, G.J. Lane, I.Y. Lee, F.S. Stephens, C.E. Svensson, K.Vetter, D. Ward, Phys. Rev. C 61 (2000) 041303(R).

[91] P. Vogel, Nucl. Phys. A 662 (2000) 148.

[92] H. Noto, Y. Abe, J. Hiura, H. Tanaka, Prog. Theor. Phys. 55 (1976) 1432.

[93] S. Marcos, H. Flocard, P.H. Heenen. Nucl. Phys. A 410 (1983) 125.

[94] P. Bonche, S. J. Krieger, M.S. Weiss, J. Dobaczewski, H. Flocard, P.-H. Heenen, Phys. Rev. Lett. 66 (1991) 876.

[95] J. Meyer, P. Bonche, M.S. Weiss, J. Dobaczewski, H. Flocard, P.-H. Heenen, Nucl. Phys. A 588 (1995) 597.

[96] J.L. Egido, L.M. Robledo, Nucl. Phys. A 524 (1991) 65.

	Oblate	Spherical	Prolate
^{64}Ge			g.s. $\beta, \gamma = 0.27, 25°$ (triaxial) $\beta_3 = 0.0$ $\Delta_p = 1.25, \Delta_n = 1.12$
^{68}Se	g.s. $\beta, \gamma = 0.28, 60°$ $\beta_3 = \beta_{33} \approx 0.08$ $\Delta_p = 1.28, \Delta_n = 1.13$		0.52 $\beta, \gamma = 0.26, 0°$ $\beta_3 = 0.0$ $\Delta_p = 1.29, \Delta_n = 1.15$
^{72}Kr	g.s. $\beta, \gamma = 0.32, 60°$ $\beta_3 = 0.0$ $\Delta_p = 1.03, \Delta_n = 1.23$		0.92 $\beta, \gamma = 0.40, 0°$ $\beta_3 = 0.0$ $\Delta_p = 1.25, \Delta_n = 0.92$
^{76}Sr	1.79 $\beta, \gamma = 0.30, 60°$ $\beta_3 = \beta_{33} \approx 0.0$ $\Delta_p = 1.47, \Delta_n = 1.43$		g.s. $\beta, \gamma = 0.51, 0°$ $\beta_3 = 0.0$ $\Delta_p = 0.67, \Delta_n = 0.50$
^{80}Zr	0.86 $\beta, \gamma = 0.20, 60°$ $\beta_3 = 0.0$ $\Delta_p = 1.02, \Delta_n = 0.82$	1.01 $\beta, \gamma = 0.0, 0°$ $\beta_3 = \beta_{32} \approx 0.15$ $\Delta_p = 0.68, \Delta_n = 0.39$	g.s. $\beta, \gamma = 0.51, 0°$ $\beta_3 = 0.0$ $\Delta_p = 0.79, \Delta_n = 0.78$
^{84}Mo	0.20 $\beta, \gamma = 0.16, 60°$ $\beta_3 = 0.0$ $\Delta_p = 1.46, \Delta_n = 1.42$	g.s. $\beta, \gamma = 0.0, 0°$ $\beta_3 = \beta_{30} \approx 0.0$ $\Delta_p = 0.74, \Delta_n = 0.72$	1.52 $\beta, \gamma = 0.66, 0°$ $\beta_3 = 0.0$ $\Delta_p = 0.0, \Delta_n = 0.0$

Table 1: Solutions of the HFB equations for proton-rich $N = Z$ nuclei in the $A = 64 - 84$ region. For each nucleus, numbers in the first line indicate excitation energies measured from the ground state. The symbol $\approx$ indicates that the potential energy curve is extremely shallow about the equilibrium value. Pairing gaps Δ_p and Δ_n are here defined as averages of diagonal elements $\Delta_{i\bar{i}}$ over 5 MeV interval around the Fermi surface, and their values (in MeV) at the equilibrium deformations are listed.

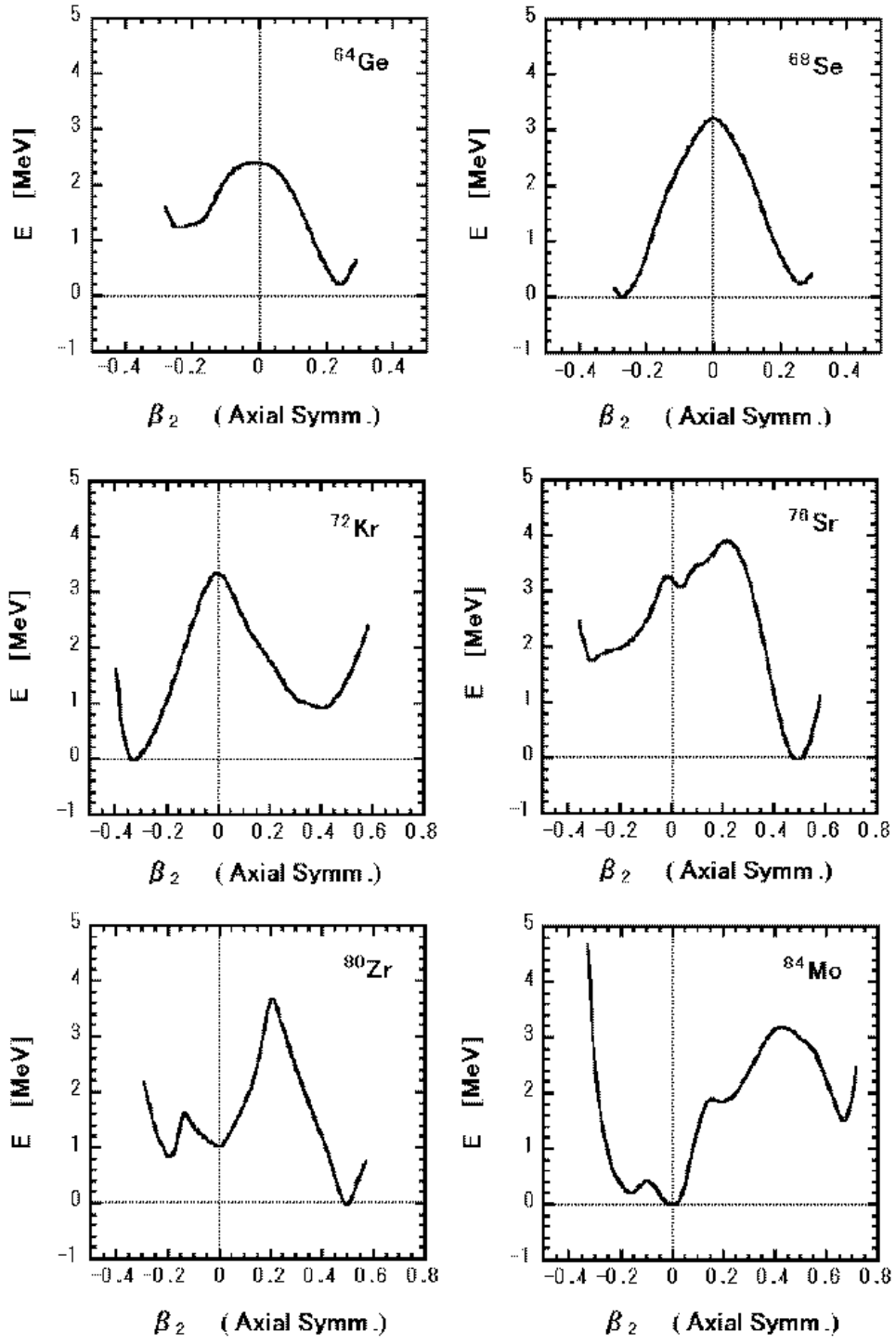

Figure 1: Potential energy curves calculated by the constrained Skyrme-HFB method for ^{64}Ge, ^{68}Se, ^{72}Kr, ^{76}Sr, ^{80}Zr and ^{84}Mo are drawn as functions of the quadrupole deformation parameter β_2. The SIII interaction is used for the particle-hole channel, while the density-dependent pairing interaction with $V_0 = -1000.0$ MeV·fm^3 and $\rho_c = 0.16$ fm^{-3} is used for the particle-particle channel.

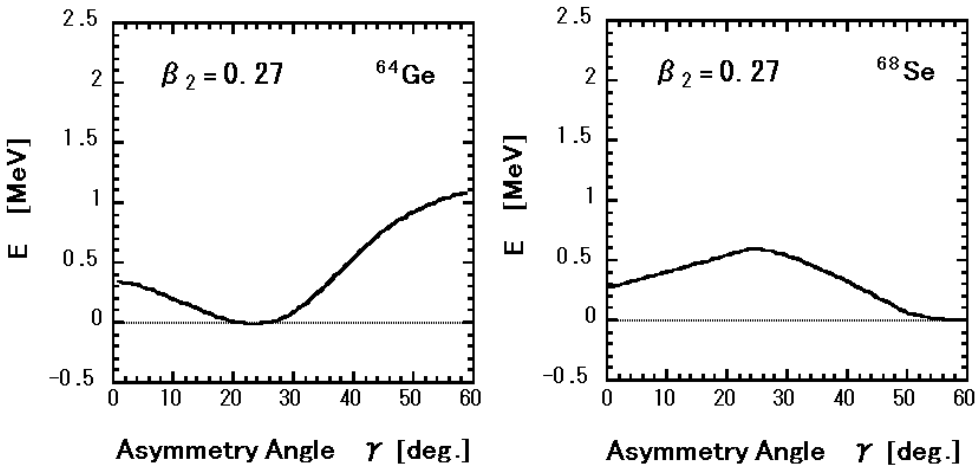

Figure 2: Potential energy curves calculated at fixed β_2 by the constrained Skyrme-HFB method for ^{64}Ge and ^{68}Se are drawn as functions of the triaxial deformation parameter γ. The effective interactions used are the same as in Fig. 1.

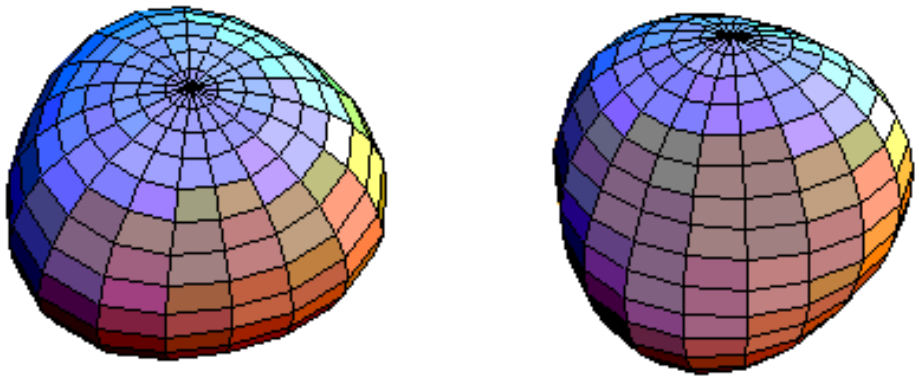

Figure 3: Density contour surfaces at the half central density of the Skyrme-HFB solution with the oblate plus triangular shape ($\beta_2 = -0.28, \beta_{33} = 0.08$) for ^{68}Se (left-hand side) and that with the tetrahedral shape ($\beta_2 = 0.00, \beta_{32} = 0.15$) for ^{80}Zr (right-hand side), listed in Table 1.

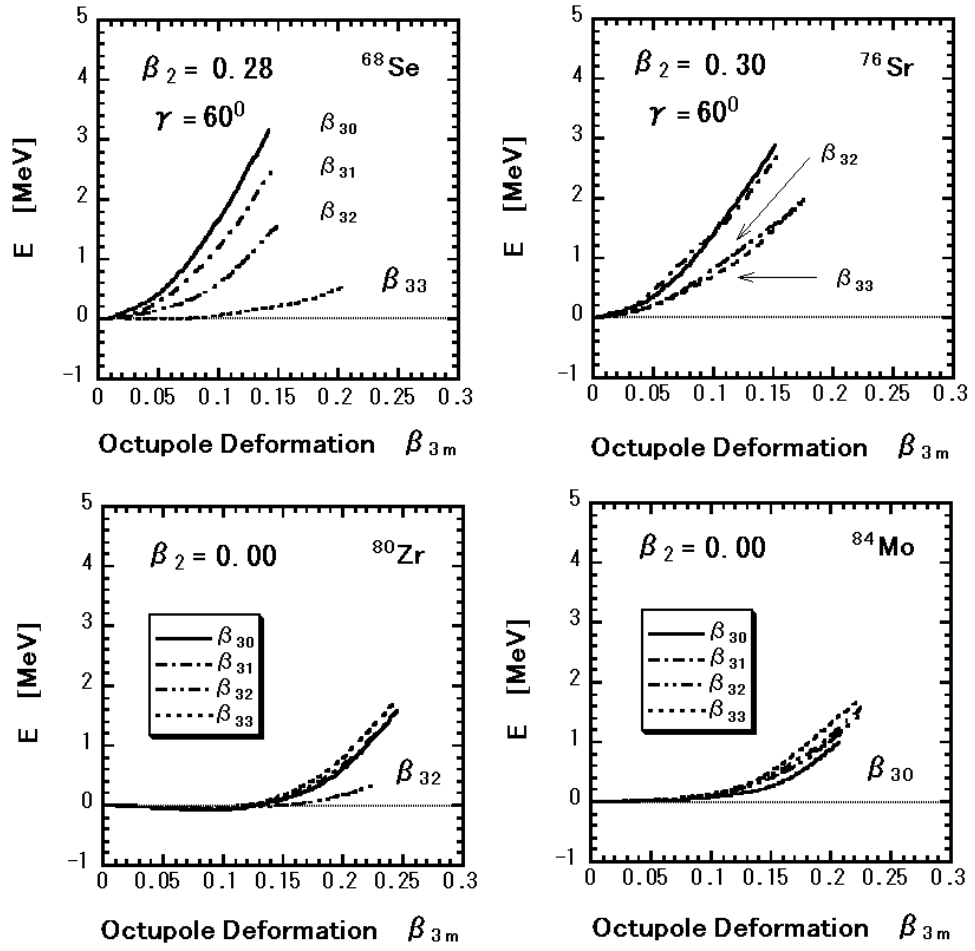

Figure 4: Potential energy curves calculated by the constrained Skyrme-HFB method are drawn as functions of the octupole deformation parameters $\beta_{3m}(m = 0, 1, 2, 3)$ about the oblate shape for ^{68}Se and ^{76}Sr, and about the spherical shape for ^{80}Zr and ^{84}Mo. One of the $\beta_{3m}(m = 0, 1, 2, 3)$ is varied while the other β_{3m}'s are fixed to zero. The effective interactions used are the same as in Fig. 1.

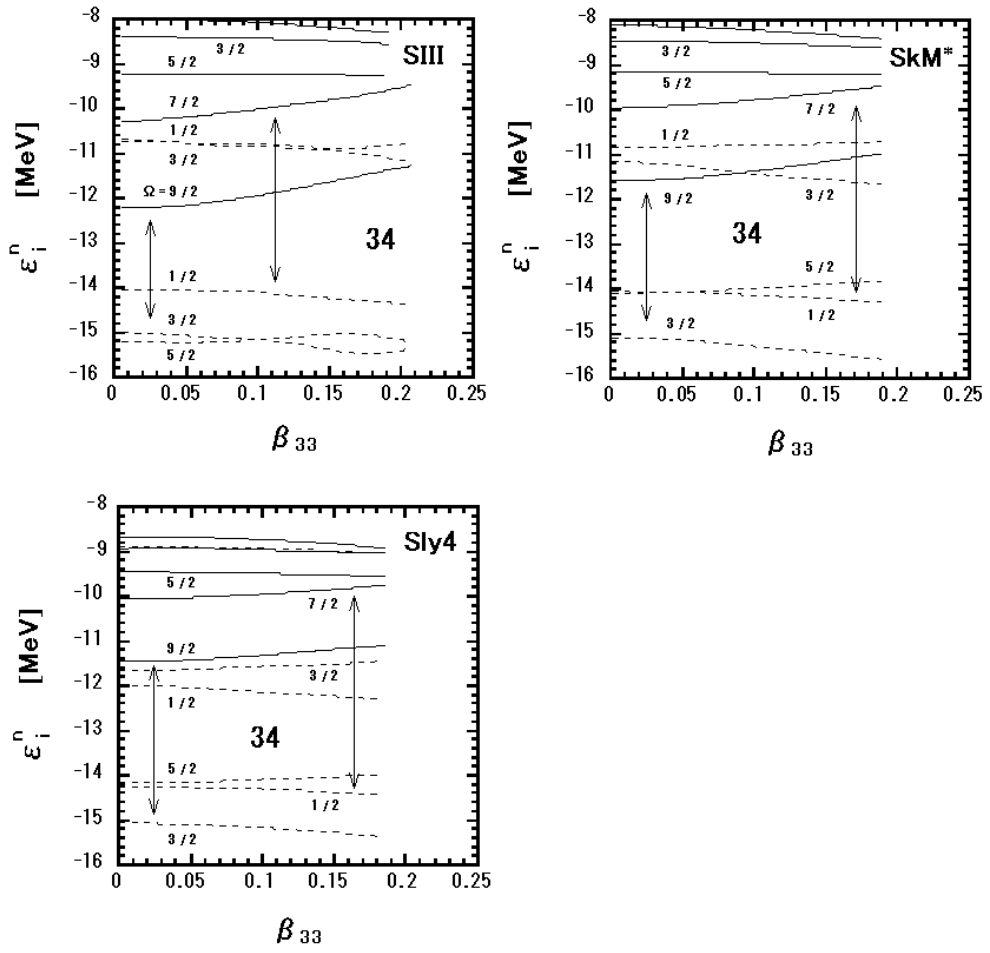

Figure 5: Neutron single-particle energies for ^{68}Se plotted as functions of the octupole deformation parameter β_{33} about the oblate shape. Here, the single-particle energies mean eigenvalues of the HF Hamiltonian with the density $\rho(\boldsymbol{r})$ determined by the HFB equations. Results for the SIII, SkM* and SLy4 parameter sets are compared. Equilibrium quadrupole deformations obtained for each Skyrme interaction are $\beta_2 = -0.28, -0.25$ and -0.24 for SIII, SkM* and SLy4, respectively. Solid (broken) lines indicate levels which have positive (negative) parity in the limit $\beta_{33} = 0$. The projection of the angular momentum on the symmetry axis, Ω, is a good quantum number only at $\beta_{33} = 0$. The arrows indicate the $\Delta\Omega = 3$ coupling associated with the triangular Y_{33} deformation as discussed in the text. The single-particle spectrum for protons is almost the same as for neutrons.

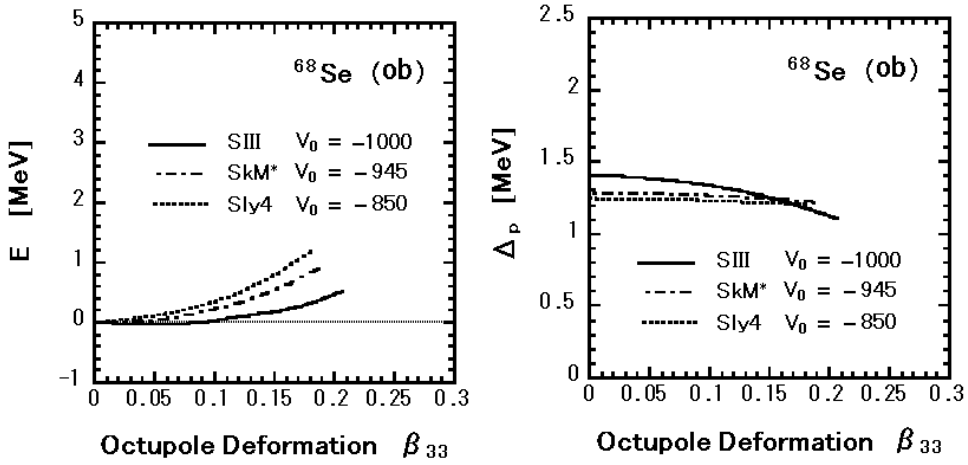

Figure 6: Comparison of the HFB potential energy curves for ^{68}Se about the oblate shape as functions of the triangular deformation parameter β_{33}, calculated for different versions of the Skyrme interaction (left-hand side). The pairing-interaction strengths V_0 are chosen such that the average pairing gaps become approximately equal for all Skyrme interactions (as displayed in the right-hand side). The calculated deformation parameter β_2 are $-0.28, -0.25$ and -0.24 for the SIII, SkM* and SLy4 interactions, respectively.

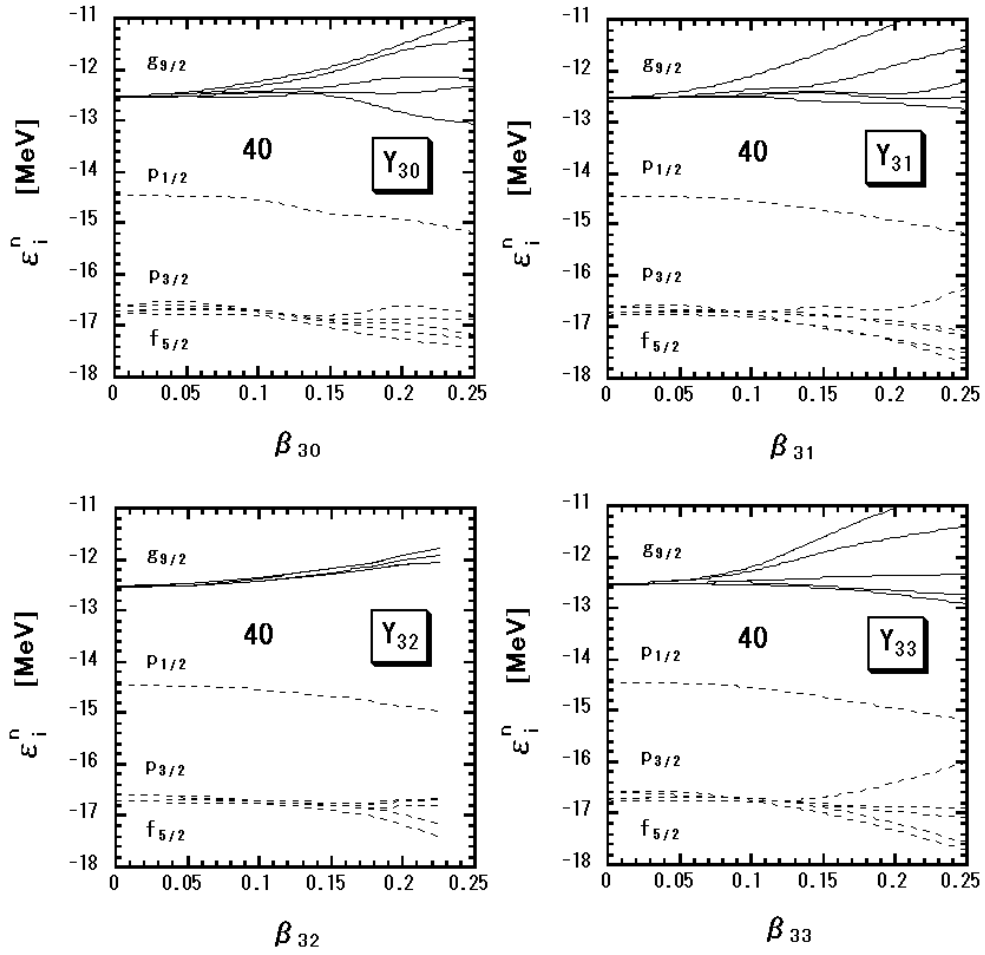

Figure 7: Neutron single-particle energies for ^{80}Zr plotted as functions of the octupole deformation parameters $\beta_{3m}(m = 0, 1, 2, 3)$ about the spherical shape. Here, the single-particle energies mean eigenvalues of the HF Hamiltonian with the density $\rho(\boldsymbol{r})$ determined by the HFB equations. The SIII interaction is used. Solid (broken) lines indicate levels which have positive (negative) parity in the limit $\beta_{32} = 0$. The single-particle spectrum for protons is almost the same as for neutrons.

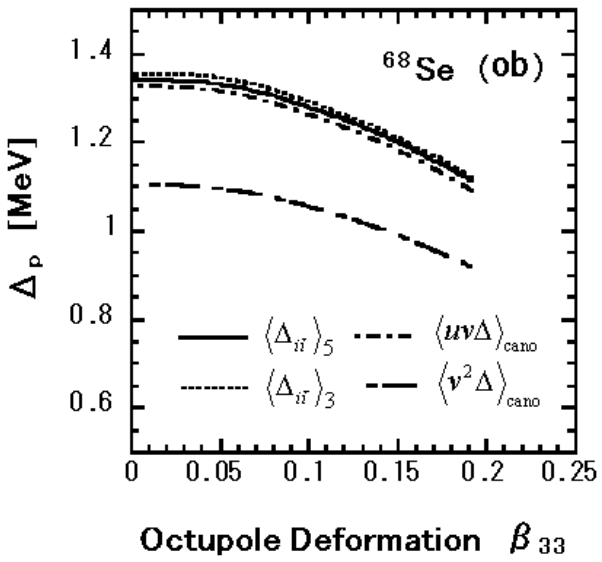

Figure 8: Comparison of differently defined average pairing gaps for ^{68}Se, plotted as functions of the triangular deformation parameter β_{33} superposed on the oblate shape. Here, $\langle\Delta_{i\bar{i}}\rangle_{\Delta E} = \sum_i f_i f_{\bar{i}} g_i g_{\bar{i}} \Delta_{i\bar{i}} / \sum_i f_i f_{\bar{i}} g_i g_{\bar{i}}$, $\langle uv\Delta\rangle_{cano} = \sum_\alpha u_\alpha v_\alpha \langle\varphi_\alpha |\Delta| \varphi_\alpha\rangle / \sum_\alpha u_\alpha v_\alpha$ [82–84] and $\langle v^2\Delta\rangle_{cano} = \sum_\alpha v_\alpha^2 \langle\varphi_\alpha |\Delta| \varphi_\alpha\rangle / \sum_\alpha v_\alpha^2$ [7], where $f_i = (1 + \exp[(\varepsilon_i - \lambda_F - \Delta E/2)/\mu])^{-1/4}$, $g_i = (1 + \exp[(\varepsilon_i - \lambda_F + \Delta E/2)/\mu])^{-1/4}$ with $\Delta E = 3$ or 5 MeV.

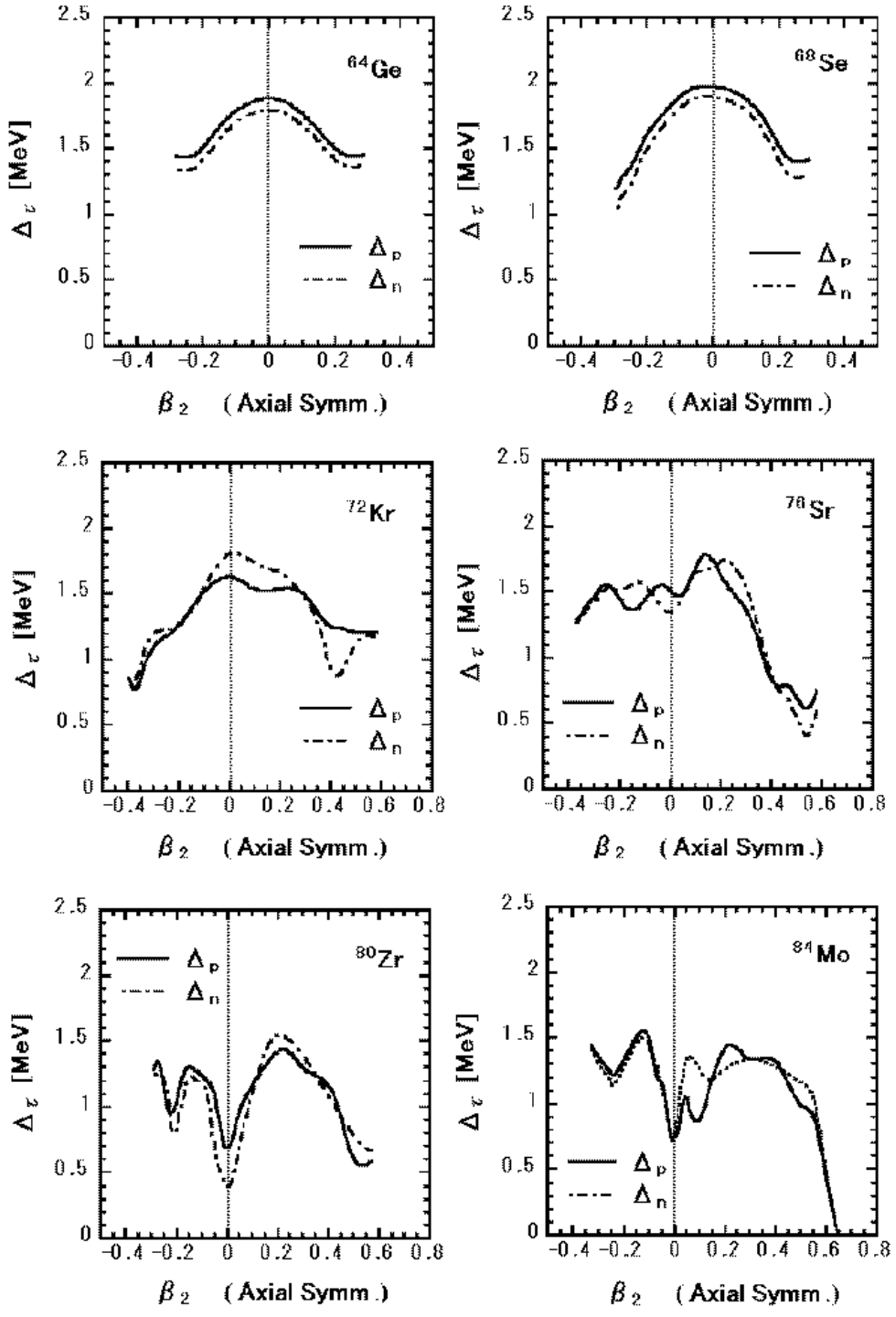

Figure 9: Variations of the pairing gaps Δ_τ (τ= p, n) calculated by the constrained Skyrme-HFB method as functions of the quadrupole deformation parameter β_2 for ^{64}Ge, ^{68}Se, ^{72}Kr, ^{76}Sr, ^{80}Zr and ^{84}Mo. The effective interactions used are the same as in Fig. 1.

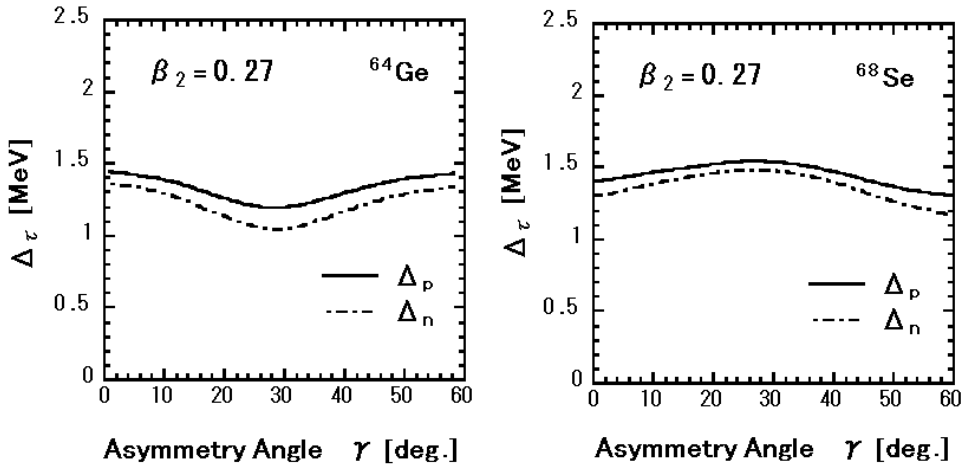

Figure 10: Variations of the pairing gaps Δ_τ (τ = p, n) calculated by the constrained Skyrme-HFB method as functions of the triaxial deformation parameter γ at fixed β_2 for ^{64}Ge and ^{68}Se. The effective interactions used are the same as in Fig. 1.

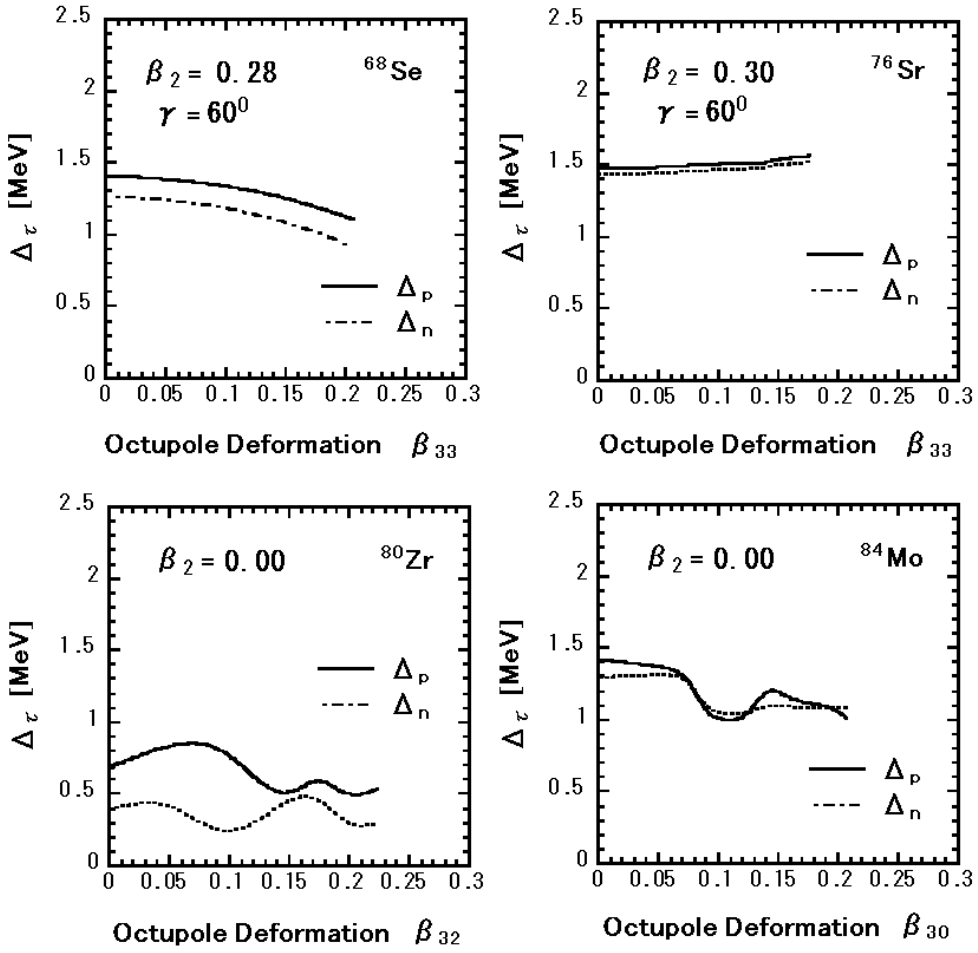

Figure 11: Variations of the pairing gaps Δ_τ (τ= p, n) calculated by the constrained Skyrme-HFB method as functions of the octupole deformation parameter $\beta_{3m}(m = 0, 1, 2, 3)$ about the oblate shape for ^{68}Se, ^{76}Sr, and about the spherical shape for ^{80}Zr, ^{84}Mo. The effective interactions used are the same as in Fig. 1.

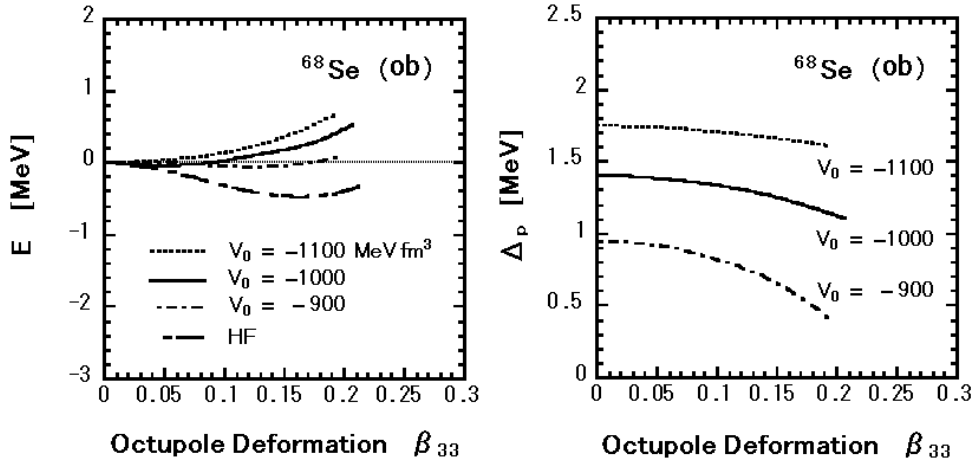

Figure 12: Comparison of the potential energy curves (left-hand side) and average pairing gaps for protons (right-hand side) calculated by the constrained Skyrme-HFB method as functions of the triangular deformation parameter β_{33} about the oblate shape for ^{68}Se with use of different strengths V_0 of the density-dependent pairing interaction (and with the same SIII interaction).